Heteroleptic Cationic Iridium(III) Complexes Bearing Phenanthroline Derivatives with Extended π-Conjugation as Potential Broadband Reverse Saturable Absorbers

Journal:	*New Journal of Chemistry*
Manuscript ID	NJ-ART-07-2019-003877.R1
Article Type:	Paper
Date Submitted by the Author:	19-Jul-2019
Complete List of Authors:	Wang, Li; Colorado State University, Chemistry; Colorado State University, Chemistry Cui, Peng; North Dakota State University, Department of Chemistry and Biochemistry Lystrom, Levi; North Dakota State University, Department of Chemistry and Biochemistry Lu, Jiapeng; North Dakota State University Kilina, Svetlana; North Dakota State University, Chemistry and Biochemistry Sun, Wenfang; North Dakota State University, Chemistry

SCHOLARONE™
Manuscripts

New J. Chem.

ARTICLE

Heteroleptic Cationic Iridium(III) Complexes Bearing Phenanthroline Derivatives with Extended π-Conjugation as Potential Broadband Reverse Saturable Absorbers

Li Wang,[a] Peng Cui,[a,b] Levi Lystrom,[a] Jiapeng Lu,[a] Svetlana Kilina[a] and Wenfang Sun[a,*]

Three cationic heteroleptic iridium(III) complexes [Ir(piq)$_2$(N^N)]$^+$ (where piq refers to 1-phenylisoquinoline and N^N represents the fluorenyl-substituted phenanthroline (phen, **1**), dipyrido-[3,2-*a*:2',3'-*c*]phenazine (dppz, **2**) and benzo[*i*]dipyrido[3,2-*a*:2',3'-*c*]phenazine (dppn, **3**)) were synthesized and their singlet and triplet excited-state characteristics were investigated via spectroscopic methods and theoretical calculations. The electronic absorption spectra of **1**-**3** in toluene all featured strongly absorbing ligand-center $^1\pi,\pi^*$ transitions below 380 nm, broad and intense diimine ligand-localized ^{1}ILCT (intraligand charge transfer) / $^1\pi,\pi^*$ transitions at 380-450 nm, weaker ^{1}LLCT (ligand-to-ligand charge transfer) / ^{1}MLCT (metal-to-ligand charge transfer) transitions at 450-520 nm, and very weak spin-forbidden ^{3}LLCT/^{3}MLCT/$^3\pi,\pi^*$ transitions at 550-680 nm. Variations of the core diimine ligand from phen to dppz caused a slight red-shift of the absorption bands at <450 nm for **2** compared to that of **1**; while changing the core diimine ligand to dppn in **3** induced a more pronounced red-shift of the bands at 380-680 nm compared to those of **1** and **2**. All three complexes exhibited structured room-temperature phosphorescence maximized at 590 nm and broad triplet excited-state absorption at 450-800 nm in toluene. However, the emission quantum yield of **3** was more than two orders of magnitude lower than those of **1** and **2** in toluene because the emitting state of **3** was the 2nd triplet excited state (T$_2$). The nature of the lowest triplet excited state (T$_1$) in toluene varied from the piq ligand localized $^3\pi,\pi^*$ mixed with some ^{3}MLCT/^{3}LMCT (ligand-to-metal charge transfer) characters in **1** and **2** to dppn ligand-based $^3\pi,\pi^*$/^{3}ILCT configuration in **3**. The different nature of the T$_1$ state in **3** resulted in a much stronger transient absorption (TA) at ca. 540 nm and 600-800 nm with a much longer TA lifetime (~23 μs). In addition, the T$_1$ state varied from pig ligand-localized $^3\pi,\pi^*$/^{3}MLCT/^{3}LMCT in toluene to dppz localized $^3\pi,\pi^*$/^{3}ILCT state in CH$_3$CN for **2**, which resulted in a shorter triplet lifetime, reduced emission quantum yield, but stronger TA signals in the NIR regions for **2** in CH$_3$CN Because of the strong triplet excited-state absorption of **1**-**3** at 532 nm, all three complexes manifested strong reverse saturable absorption (RSA) at 532 nm, with the RSA trend following **3**>**2**>**1**. Fluorenyl substitution not only enhanced the RSA at 532 nm for **2** and **3**, but also made them potential broadband reverse saturable absorbers.

Introduction

Organometallic d$_6$ transition-metal complexes have drawn great interest in the past two decades. Particularly, Ir(III) complexes are considered to be one of the most promising metal complexes because they exhibit: 1) good photo- and thermal stability;[1] 2) high quantum yield for triplet excited-state formation due to the large spin-orbit coupling constant of Ir(III) ion;[2] 3) facile colour tuning ability through ligand structural modification;[3] 4) long-lived triplet excited states.[4] Among these features, the large spin-orbit coupling constant is the most attractive feature for Ir(III) complexes to be used as the emitting layer in organic light emitting diodes (OLEDs)[5,6] and light-emitting electrochemical cells (LEECs)[7] because it enables almost quantitative population of the triplet excited state and

thus improves the phosphorescence efficiency. In addition, facile generation of triplet excited states in the Ir(III) complexes facilitates their applications as sensitizers for charge-transfer reactions in DNA,[8,9] photocatalytic CO$_2$ reduction,[10] triplet-triplet annihilation-based photon upconversion,[11,12] and photodynamic therapy (PDT).[13-18]

Despite the diverse applications mentioned above, exploration of the nonlinear optical properties and the optical limiting effects based on reverse saturable absorption of the Ir(III) complexes have been quite limited.[19-34] Reverse saturable absorption (RSA) refers to the nonlinear optical phenomenon in which the absorptivity of the materials increases with the increased incident fluence because of the stronger excited-state absorption than the ground-state absorption.[35-37] The strength of RSA of a material is mainly determined by the ratio of the excited-state absorption cross section (σ_{ex}) relative to that of the ground-state (σ_0).[38] Meanwhile, the excited-state quantum yield and lifetime also impact the excited-state absorption. Therefore, in order to maximize the RSA at a given wavelength,

[a]Department of Chemistry and Biochemistry, [b]Materials and Nanotechnology Program, North Dakota State University, Fargo, North Dakota, 58108-6050, USA.

large σ_{ex}/σ_0 ratio, high excited-state quantum yield, and long-lived excited state are needed.

In our previous work,[15,19,21,23-26,28-31] we have mainly focused on studying the RSA of the cyclometalated monocationic Ir(III) complexes Ir(N^N)(C^N)$_2$$^+$ (where N^N refers to the diimine ligand and C^N refers to the cyclometalated ligand). We have demonstrated that modifications of either the cyclometalated ligand (C^N) or the diimine ligand (N^N) influenced the photophysical properties and the RSA performance of the Ir(III) complexes drastically. Particularly, we found that expanding the π-conjugation of the N^N ligand by introducing π-conjugated substituents extended the triplet excited-state absorption to the near-infrared (NIR) region without sacrificing the transparency of the Ir(III) complexes in the visible to the NIR regions.[23] Meanwhile, the triplet excited-state lifetimes of the complexes were significantly increased. On the contrary, expanding the π-conjugation of the N^N ligand via benzannulation at appropriate site of the N^N ligand red-shifted the very weak spin-forbidden $^3\pi,\pi*/^3$CT (charge transfer) absorption band while shortened the triplet excited-state lifetimes of the Ir(III) complexes.[30] For broadband optical limiting applications, it is very important to red-shift both the ground- and excited-state absorption and maintain large ratios of σ_{ex}/σ_0 in the visible to the NIR regions as well as keep a long-lived triplet excited state.

Among the variety π-conjugated N^N ligands, phenanthroline (phen) and its derivatives, such as dipyrido[3,2-a:2',3'-c]phenazine (dppz) and benzo[i]dipyrido[3,2-a:2',3'-c]-phenazine (dppn) were among the most studied ligands. It has been well demonstrated that Ru(II) complexes with the formula of [Ru(bpy)$_2$(dppn)]$^{2+}$ (where bpy refers to 2,2'-bipyridine) and Ir(III) complexes of the Ir(C^N)$_2$(dppn)$^+$ type possessed strongly absorbing and long-lived dppn-localized $^3\pi,\pi*$ states.[15,39,40] Because the triplet excited-state absorption of the dppn $^3\pi,\pi*$ state maximized at ca. 530 nm, the Ir(III) complexes bearing the dppn ligands all gave rise to very strong RSA at 532 nm for ns laser pulses.[15] However, the ground-state absorption of the Ir(piq)$_2$(dpq)$^+$, Ir(piq)$_2$(dppz)$^+$ and Ir(piq)$_2$(dppn)$^+$ complexes with cyclometalating 1-phenylisoquinoline (piq) ligands was limited to shorter than 600 nm, and the excited-state absorption of these complexes in the NIR region is weak.

To broaden the ground-state absorption to the longer wavelength and enhance the triplet excited-state absorption in the NIR region while keeping a long-lived triplet excited state for broadband optical limiting applications, we synthesized three monocationic Ir(III) complexes bearing fluorenyl substituted phen, dppz or dppn as the diimine ligand. The structures of the three complexes are shown in Chart 1. The synthesis, photophysics, and RSA of **2** and **3** are reported in this work. Although complex **1** has been reported in our previous work,[25] it is included in this work for comparison purpose.
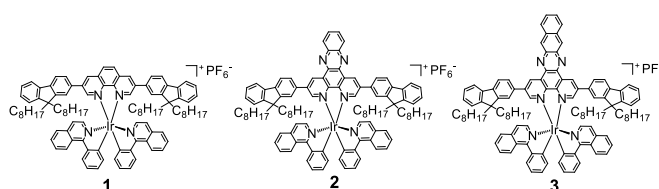

Chart 1 Molecular structures of Ir(III) complexes **1**-**3**.

Results and discussion

Synthesis

The synthesis and characterization of complex **1** was reported by our group previously.[25] For synthesizing the fluorenyl-substituted dppz ligand for complex **2**, we followed the procedure reported by Yagi, in which a similar ligand was used for a platinum complex.[41] As depicted in Scheme 1, oxidation of 3,8-dibromo-1,10-phenanthroline (phenBr2) gave the dione intermediate (phenBr2O2) with a moderate yield of 46%. Then a condensation reaction of the dione and o-phenylenediamine gave the dibrominated intermediate dppz-2Br with a yield of 88%. Finally, Suzuki-Miyaura coupling of dppz-2Br with 2-(9,9-bis(2-ethylhexyl)-9H-fluoren-2-yl)-4,4,5,5-tetramethyl-1,3,2-dioxaborolane (F8-borate) in a mixed solvent of 1,2-dimethoxyethane (DME), ethanol and water gave the fluorenyl-substituted dppz (**L2**) as a pale yellow oil. Complex **2** was synthesized by refluxing **L2** with chlorobis(1-phenylisoquinoline)iridium(III) dimer in dichloromethane (DCM) / MeOH (2/1) with the aid of silver salt.

For preparing complex **3**, we first attempted to synthesize the fluorenyl-substituted dppn ligand using the similar procedure described for **L2**. The condensation reaction of phenBr$_2$O$_2$ with 2,3-diaminonaphthalene gave a brownish powder (dppn-2Br) with nearly a quantitative yield, which showed very limited solubility in common organic solvents (chloroform, DMSO, THF, toluene). Then Suzuki-Miyaura coupling reaction of dppn-2Br with F8-borate was attempted. Unfortunately, after 48-hour refluxing, the obtained product was almost quantitative dppn ligand. Thus, under the Suzuki-Miyaura coupling reaction condition, dppn-2Br would be debrominated. We then reversed the reaction sequence by attaching the fluorenyl substituents to the dione derivative phenBr2O2 first and subsequently conducting the condensation reaction on the fluorenyl substituted phenanthroline dione. However, phenBr2O2 readily decomposed under the basic condition that is required for the Suzuki-Miyaura coupling reaction.[42,43] The dione group was then protected using 2-nitropropane in CH$_3$CN/H$_2$O to give a brownish-yellow amorphous solid.[42,44,45] After that, the protected phenBr2O2X was used to couple with F8-borate under Suzuki-Miyaura coupling reaction condition, but no reaction occurred after 48 hours. Almost all of the phenBr2O2X was recycled. Therefore, the attempt following the Rau's method also failed.[45]

At last, we turned to the 'chemistry-on-the-complex' approach, which has been proven to be efficient for ligands that are hard to be accessed because of the limited solubility of the ligands.[46] Starting from dppn-2Br and chlorobis(1-

ARTICLE

phenylisoquinoline)iridium(III) dimer, similar procedure was followed as the synthesis of complex **2**. Initially, the ligand dppn-2Br did not dissolve in dichloromethane/MeOH at room temperature, however, the suspension finally turned into clear red solution after refluxing for 24 hours. After separation, the complex Ir(piq)$_2$(dppn-2Br) was obtained as a red powder. Then Suzuki-Miyaura coupling reaction with F8-borate gave the final

complex **3** with a moderate yield of 33%. The final complexes **1-3** were characterized with ^{1}H-NMR, HRMS and elemental analyses (ESI, Figs. S1-S5). All three complexes dissolved well in dichloromethane, acetonitrile, chloroform, toluene, and in hot hexane due to incorporation of the fluorenyl substituent to the N^N ligand.
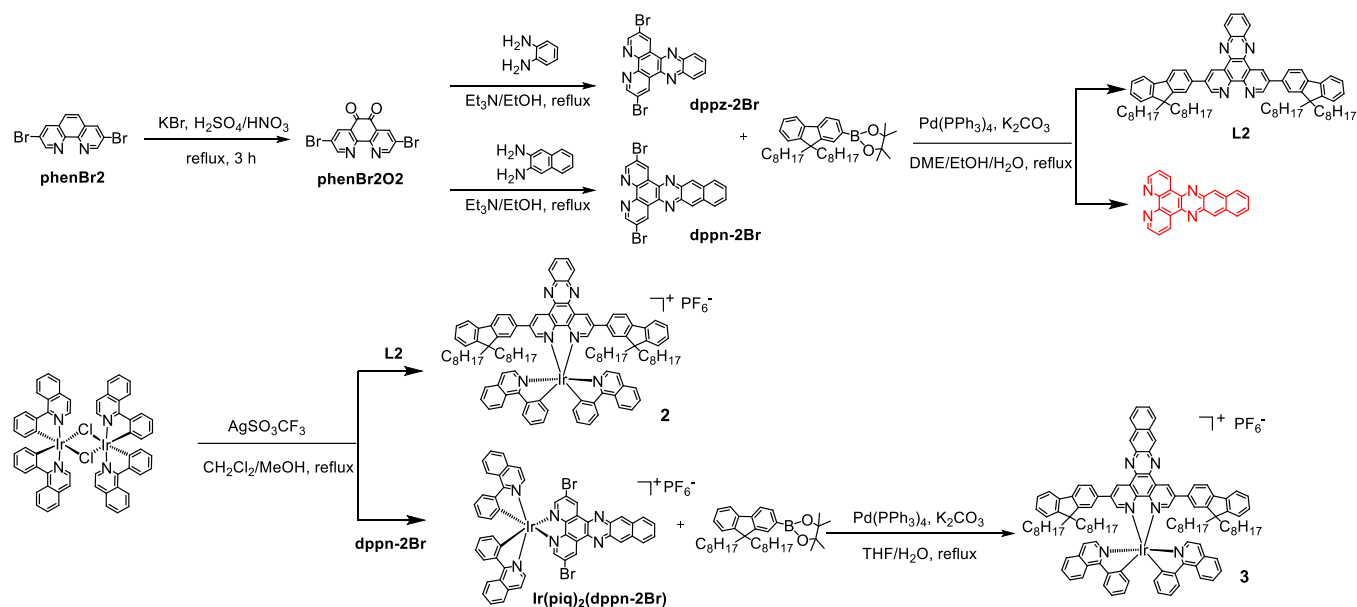
Scheme 1 synthetic routes for complexes **2** and **3**.

UV-vis absorption

The UV-vis absorption of complexes **1-3** was measured in CH$_3$CN, CH$_2$Cl$_2$, and toluene. The absorption spectra in toluene are displayed in Fig. 1, and the band maxima and molar extinction coefficients are summarized in Table 1. For better understanding the impact of fluorenyl substitution on the absorption spectra of complexes **2** and **3**, the spectra of these two complexes in CH$_3$CN were compared to their corresponding complexes Ir(piq)$_2$dppz and Ir(piq)$_2$dppn without the fluorenyl substituents on the diimine ligands in CH$_3$CN (because Ir(piq)$_2$dppz and Ir(piq)$_2$dppn have poor solubility in toluene) (ESI, Fig. S6). For all three complexes, the obedience of the Beer's law in the concentration range used in our study (5×10^{-6} - 1×10^{-4} mol·L^{-1}·cm^{-1}) indicates the absence of ground-state aggregation in the studied concentration range. All three complexes exhibited minor solvatochromic effect, as reflected by the similar spectral feature and transition energies in solvents with different polarities, such as CH$_3$CN, toluene and CH$_2$Cl$_2$ (Fig. S7).

As shown in Fig. 1, the absorption spectra of **1** - **3** can be divided into four regions: the strong absorption band(s) below 365 nm, the broad and strong absorption bands at 380-450 nm, the relatively weaker absorption bands at 450-520 nm, and the very weak absorption band(s) that were only visible in the expanded spectra at 550-680 nm (see the inset in the upper panel of Fig. 1). Considering the transition energies, molar

extinction coefficients, spectral features, and with reference to the absorption spectra of the corresponding complexes Ir(piq)$_2$dppz and Ir(piq)$_2$dppn,[15] the < 365 nm band(s) can be attributed to the ligand-centered $^1\pi,\pi^*$ transitions mixed with some ligand-to-ligand charge transfer (^{1}LLCT) / metal-to-ligand charge transfer (^{1}MLCT) characters; while the 380-450 nm bands are dominated by the diimine ligand-localized intraligand charge transfer (^{1}ILCT) / $^1\pi,\pi^*$ transitions. The relatively weaker absorption bands at 450-520 nm could be dominated by the ^{1}LLCT/^{1}MLCT transitions. However, the much larger ε values in **3** imply that $^1\pi,\pi^*$/^{1}ILCT transition from the diimine ligand could likely contribute. The very weak absorption band(s) at 550-680 nm can be attributed to the spin-forbidden ^{3}LLCT/^{3}MLCT/$^3\pi,\pi^*$ transitions. These assignments are well supported by the time-dependent density functional theory (TDDFT)[47-50] calculation results (see natural transition orbitals (NTOs)[51] in Tables 2 and S1, and the compared experimental and calculated spectra for each complex in Fig. S8).

Table 1 Photophysical data for complexes **1-3** in toluene

	λ_{abs}/nm (ε/10^4 L.mol^{-1}.cm^{-1})	λ_{em}/nm (τ_{em}/μs; Φ_{em}	λ_{T1-Tn}/nm (τ_T/μs; ε_{T1-Tn}/10^3 L.mol^{-1}.cm^{-1}); Φ_T^b
1^a	334 (5.50), 359 (4.76), 386 (5.15), 405 (4.35), 470 (sh., 0.53), 570 (0.02)	590 (3.1), 623 (3.1); 0.46	523 (3.2; 5.40); 0.15

2	338 (5.12), 353 (5.16), 373 (5.16), 397 (5.53), 420 (4.52), 482 (sh., 0.48), 567 (0.023)	590 (2.9), 623 (2.9); 0.40	525 (2.9; 5.90); 0.31
3	331 (7.86), 404 (4.34), 424 (4.01), 461 (sh., 1.23), 492 (sh., 0.50), 567 (0.023), 632 (0.006)	590 (2.0), 623 (1.8); 0.003	380 (22.9, -), 542 (22.9, 8.65), 755 (24.0, 2.11); 0.29

[a] From Ref. 25. [b] The ε_{T1-Tn} and Φ_T values were determined by partial saturation method.[52,53]
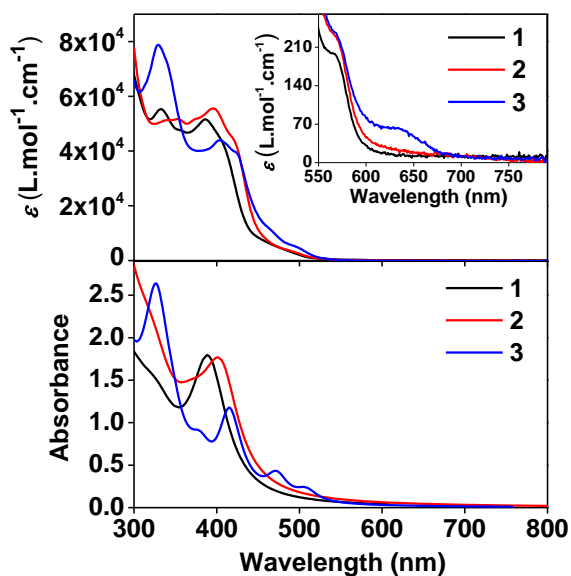

Fig. 1 Comparison of the experimental (top) and the calculated (bottom) absorption spectra of complexes **1-3** in toluene at room temperature. The calculation was carried out using the PBE1 functional.

Table 2 Natural transition orbitals (NTOs) representing the major singlet transitions contributing to the low-energy absorption bands of **1-3** in toluene.

	Excited states and properties	Hole	Electron
1	S_1 424 nm $f = 0.005$		
2	S_1 424 nm $f = 0.003$		
3	S_1 514 nm $f = 0.001$		
	S_2 508 nm $f = 0.140$		
	S_3 472 nm $f = 0.270$		

Changing the diimine ligand from phen in **1** to dppz in **2** only caused a slight red-shift of the absorption bands below 450 nm. In contrast, changing the diimine ligand to dppn in **3** saliently red-shifted all of the absorption bands at > 380 nm compared to those of **1** and **2**, accompanied by a significantly enhanced absorption of the 331-nm band and the appearance of a very weak absorption band at 632 nm. However, this weak band in **3** is only observed in toluene but not in acetonitrile (Fig. S6). Comparison of the absorption spectra of **1**-**3** to their corresponding complexes without the fluorenyl substituents revealed that the major impact of the fluorenyl substitution at the diimine ligands was the induction of the ^{1}ILCT transition at ca. 420 nm, which drastically increased the molar extinction coefficients for the 380-450 nm bands in **1**-**3**.

Emission

The emission characteristics of **1-3** were studied in toluene, CH_3CN and CH_2Cl_2, and the normalized spectra are presented in Figs. 2 and S9. Emission band maxima, lifetimes and quantum yields are summarized in Tables 1 and S2. All three complexes showed orange-red luminescence after exciting at their respective major absorption bands. The observed emission is assigned to phosphorescence based on the following facts: (1) the emission spectra of **1-3** were significantly red-shifted in comparison to their corresponding excitation wavelength (405 nm for **1**, 420 nm for **2**, and 424 nm for **3** in toluene); (2) the emission lifetimes were long (2-3 μs, see Tables 1 and S2); and (3) the emission is prone to oxygen quenching. Solvent had a minor effect on the emission energies of **1-3** (ESI, Fig. S9). The minor solvatochromic effect along with the vibronic structure in the emission spectra suggest that the emitting states likely to be associated with the ligand-localized ${}^3\pi,\pi^*$ state. However, despite the almost identical emission energies for **1-3**, the emission quantum yields of **1** (46%) and **2** (40%) were more than two orders of magnitude larger than that of **3** (0.3%). This dramatic difference implies that the nature of the emitting state for **3** could be different from those of **1** and **2**. In addition, the emission lifetime was much shorter and the emission quantum yield was much lower in CH_3CN than in toluene and CH_2Cl_2 for **2**, which implies a possible change of the nature of the lowest triplet excited state in CH_3CN for **2** and has been confirmed by the TDDFT calculation results (Tables 3 and S3) being discussed in the following paragraph, and will be further discussed in the transient absorption section *vide infra*.

To unambiguously understand the nature of the emitting states for **1-3**, analytical gradient TDDFT calculations[54,55] were carried out by optimizing the triplet excited-state geometries. The NTOs representing the low(est)-energy triplet transitions of **1-3** in toluene are depicted in Table 3. The calculated energies for T_1 of **1** and **2** and T_2 of **3** are the same, and the natures of these states are all piq ligand-localized ${}^3\pi,\pi^*$ states mixed with some ^{3}MLCT/^{3}LMCT (ligand-to-metal charge transfer) characters. This trend is consistent with the experimental emission results even if the calculated energies are underestimated. Although the energy and electronic configuration of the T_2 state of **3** are identical to the T_1 states of **1** and **2**, its non-lowest excited state nature results in the much

ARTICLE

lower emission efficiency of **3**. In addition, the NTOs of T_1 state of **2** in CH_3CN (ESI Table S3) changed to the dppz core ligand-localized $^3\pi,\pi^*$/^{3}ILCT configuration, which accounted for the pronouncedly reduced emission lifetime and quantum yield of **2** in CH_3CN compared to those in toluene.
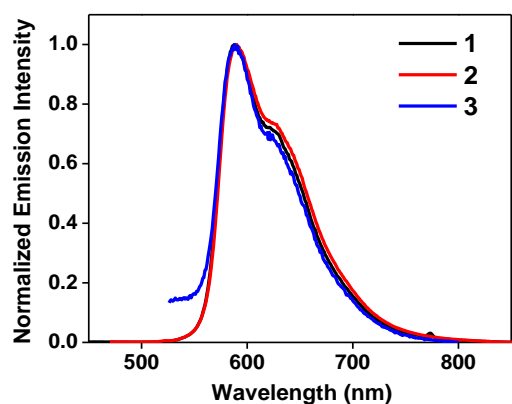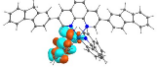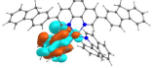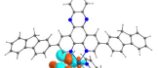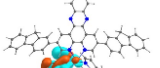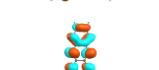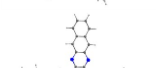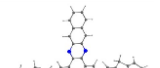

Fig. 2 Normalized emission spectra of complexes **1-3** in toluene at room temperature. λ_{ex} = 405 nm for **1**, 420 nm for **2**, and 424 nm for **3**.

Table 3 Natural transition orbitals (NTOs) of the low(est)-energy triplet transitions of **1-3** in toluene.

	T_n energy	Electron	Hole
1	T_1 896 nm		
2	T_1 896 nm		
3	T_1 950 nm		
	T_2 896 nm		

Transient absorption (TA)

The triplet excited-state absorption of **1-3** in degassed toluene and CH_3CN solutions was investigated by nanosecond transient absorption (TA) spectroscopy. The TA absorption band maxima, excited-state lifetimes obtained from the decay of the TA signals, and the triplet molar extinction coefficients and quantum yields deduced from the partial saturation method[52,53] for **1-3** in toluene are listed in Table 1. The TA spectra at zero-delay after the 355-nm excitation for **1-3** in toluene are provided in Fig. 3, and the time-resolved spectra in toluene and acetonitrile are presented in Figs. S10 and S11 (ESI).

The TA spectra of all three complexes featured broad and intense positive absorption bands in the spectral range of 450 - 800 nm. No detectable bleaching bands for **1** and **2** were

observed in toluene. In contrast, **3** exhibited a bleaching centered at 431 nm. The TA spectra of **1** and **2** in toluene were quite similar to each other, and both resembled the spectrum of the $[Ir(piq)_2Cl]_2$ dimer (see Fig. S12, ESI). In addition, the triplet lifetimes of **1** (3.2 μs) and **2** (2.9 μs) in toluene were quite similar, and consistent with their emission lifetimes (see Table 1) in the same solvent. These features suggest that the observed transient absorption for **1** and **2** in toluene emanates from the same structural component in these two complexes, and the excited states giving rise to the observed TA should be the emitting excited states. With reference to the nature of the emitting states discussed in the previous section for **1** and **2**, the TA of **1** and **2** is attributed to the piq (C^N) ligand-localized $^3\pi,\pi^*$ state mixed with some ^{3}MLCT/^{3}LMCT characters in toluene. When measured in acetonitrile, the TA spectrum and lifetime of **1** were similar to those obtained in toluene. However, the TA spectrum of **2** in acetonitrile was somewhat different from that in toluene, with an obvious bleaching band appearing at ca. 400 nm and a new broad band emerging in the NIR region (600 – 800 nm), accompanied by a reduced lifetime of 1.06 μs. These changes together with the aforementioned significantly reduced emission quantum yield and lifetime (1.05 μs) in CH_3CN suggest a change of the nature of the lowest triplet excited state in CH_3CN. Considering the NTOs for the T_1 state of **2** in CH_3CN, we attribute the excited state giving rise to the detected TA of **2** in CH_3CN to the dppz localized $^3\pi,\pi^*$/^{3}ILCT state, which could be stabilized more than the piq ligand-localized $^3\pi,\pi^*$/^{3}MLCT/^{3}LMCT state in polar CH_3CN solvent and became the lowest triplet excited state in **2** in CH_3CN.

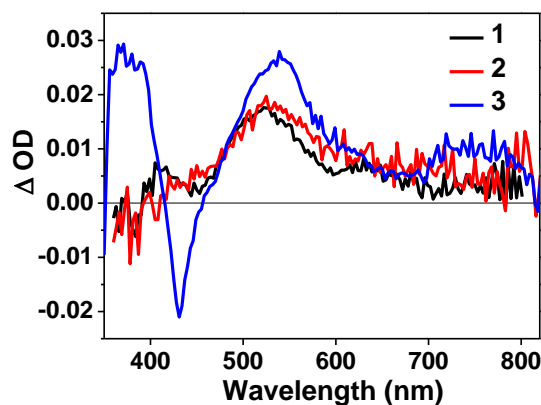**Fig. 3** TA spectra of complexes **1-3** in toluene at zero time-delay at room temperature. λ_{ex} = 355 nm, $A_{355\ nm}$ = 0.4 in a 1-cm cuvette

For complex **3**, its TA spectral feature and lifetime were quite different from those of **1** and **2** in toluene. Especially its triplet lifetime deduced from the decay of TA signals was one order of magnitude longer than its emission lifetime. This phenomenon is not unexpected in Ru(II) and Ir(III) complexes bearing dppn ligand, in which a non-emissive but long-lived dppn-ligand localized $^3\pi,\pi^*$ state that gave rise to a strong transient absorption at ca. 530 nm and a high-lying, short-lived ^{3}CT emitting state exist.[15,39,40,56] In view of the similar shape and energy of the major TA band of **3** to those of the dppn ligand[15]

and the corresponding Ir(piq)$_2$dppn complex (ESI Fig. S11), as well as the NTOs for the T$_1$ state of **3**, we attribute the observed TA to the dppn-localized $^3\pi,\pi^*$/^{3}ILCT state. The involvement of ^{3}ILCT character can be further supported by the presence of a broad NIR band maximized at ca. 740 nm in the TA spectrum of **3** compared to that of Ir(piq)$_2$dppn (ESI Fig. S13). Meanwhile, the triplet lifetime deduced from the decay of the TA signals for **3** in CH$_3$CN (20.4 μs) was shorter than that of Ir(piq)$_2$dppn (35.7 μs) in CH$_3$CN.[15] These characteristics imply that the transient absorbing excited state in **3** contain the ^{3}ILCT configuration. Comparison of the TA spectrum of **3** with that of Ir(piq)$_2$dppn, and **2** with that of (Ir(piq)$_2$dppz (Fig. S13) confirmed that introduction of the electron-donating fluorenyl substituent to the diimine ligands indeed increased the triplet excited-state absorption in the NIR region and meanwhile maintained the long triplet lifetime.

Reverse saturable absorption (RSA)

As discussed above, complexes **1-3** showed broad and positive TA at ca. 450 - 800 nm, indicating stronger triplet excited-state absorption than that of the ground state in this spectral region. Therefore, reverse saturable absorption (RSA) is expected to occur from these complexes for nanosecond laser pulses. To demonstrate this, nonlinear transmission experiments were carried out for **1-3** in toluene solution in a 2-mm cuvette using 4.1-ns, 532-nm laser pulses. The linear transmission of all complex solutions was adjusted to 80% at 532 nm in a 2-mm cuvette in order to ensure the same numbers of molecules being excited to the singlet excited state upon laser irradiation. Under this condition, the observed RSA performance would be directly correlated to the strength of the triplet excited-state absorption, which is determined by the combination of triplet excited-state absorption cross section, triplet excited-state quantum yield and lifetime. The transmission vs. incident energy curves for **1-3** are depicted in Fig. 4. To assess the impact of fluorenyl substitution at the diimine ligand on the RSA, the RSA of **2** and **3** was compared to their counterparts without the fluorenyl substituent, *i.e.* Ir(piq)$_2$dppz and Ir(piq)$_2$dppn, respectively (ESI, Fig. S14).

Fig. 4 manifests that **1-3** all exhibited very strong RSA at 532 nm, with the transmission decreased to ~21% for **1**, ~19% for **2** and ~14% for **3** when the incident fluence of the laser increased to ca. 3 J/cm^2. The RSA strength of **1-3** at 532 nm obviously followed the trend of **3>2>1**. It is well understood that the RSA strength of a compound is mainly determined by the combined ratio of the excited-state absorption cross section (σ_{ex}) with respect to that of the ground state (σ_0) and the triplet excited-state quantum yield. The ground-state absorption cross sections of **1-3** at 532 nm can be determined from the molar extinction coefficients obtained from their UV-vis absorption spectra using a conversion factor of $\sigma = 3.82\times10^{-21}\varepsilon$, while the excited-state absorption cross sections at 532 nm can be deduced from the ΔOD values at 532 nm and at the TA band maximum using the equation of ΔOD$_{532}$/ΔOD$_{max}$ = (ε_{ex}^{532}-ε_0^{532}) / (ε_{ex}^{max}-ε_0^{max}). The resultant values along with the σ_{ex}/σ_0 and $\Phi_T\sigma_{ex}/\sigma_0$ ratios are listed in Table 4. It is quite obvious that the $\Phi_T\sigma_{ex}/\sigma_0$ ratios follow the trend of **3>2>1** at 532 nm, which

parallels the observed RSA trend for these complexes. When compared to their analogues without the fluorenyl substituent, complexes **2** and **3** manifested slightly better RSA at 532 nm (Figure S14, ESI). These results confirmed the benefits of introducing π-donating fluorenyl substituent to the diimine ligands in the Ir(III) complexes. Especially considering the enhanced excited-state absorption of these complexes in the NIR region, these complexes potentiate themselves as promising candidates as broadband reverse saturable absorbers for OPL applications.

Table 4 Ground-state and excited-state absorption cross sections of complexes **1-3** in toluene

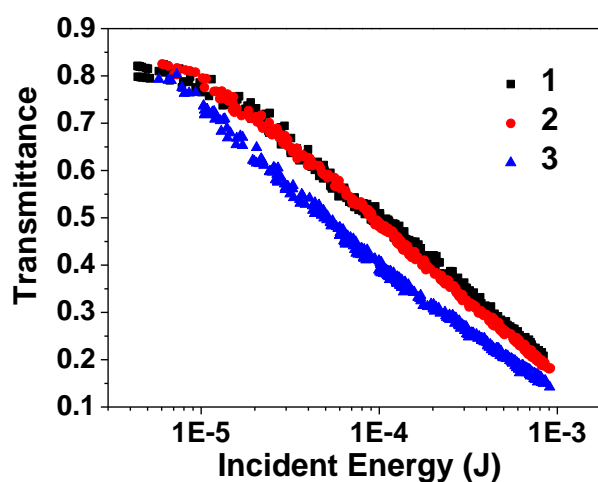|	**1**	**2**	**3**
σ_0 / 10^{-18} cm^2	1.99	2.52	3.26
σ_{ex} / 10^{-18} cm^2	18.8	20.4	33.1
σ_{ex}/σ_0	9.45	8.10	10.2
$\Phi_T\sigma_{ex}/\sigma_0$	1.42	2.51	2.94

Fig. 4 Transmittance *vs* incident energy curves for **1-3** in toluene for 4.1 ns laser pulses at 532 nm in a 2-mm cuvette. The linear transmission was adjusted to 80% for each sample in a 2-mm cuvette. The radius of the beam waist at the focal plane was approximately 96 μM.

Conclusions

We synthesized and characterized three cationic heteroleptic Ir(III) complexes **1-3** bearing fluorenyl-substituted phen, dppz and dppn as the diimine ligand, respectively. For complexes **1** and **2**, the fluorenyl substituent was incorporated to the diimine ligand phen or dppz first, then the substituted diimine ligands were used to coordinate with the chloro-bridged cyclometalated Ir(III) dimer complex [Ir(piq)$_2$Cl]$_2$. However, this synthetic strategy did not work for the synthesis of **3** because of the poor solubility of the dppn-2Br intermediate, which led to de-bromination of dppn-2Br rather than the desired substitution reaction under the Suzuki-Miyaura coupling reaction condition. At the end, the 'chemistry-on-the-complex'

approach gave the desired complex **3** with a moderate yield (33%). All three complexes possessed broad and intense diimine ligand-localized ^{1}ILCT / $^1\pi,\pi^*$ transitions at 380-450 nm, weaker ^{1}LLCT/^{1}MLCT transitions at 450-520 nm, and very weak spin-forbidden ^{3}LLCT/^{3}MLCT/$^3\pi,\pi^*$ transitions at 550-680 nm. For **3**, dppn-localized $^1\pi,\pi^*$ and ^{1}ILCT (π(fluorenyl)$\rightarrow \pi^*$(dppn)) also contributed significantly to the 450-520 nm bands. Variation of the core diimine ligand from phen or dppz to dppn caused a pronounced red shift of all of the aforementioned absorption bands in **3**; while changing the core ligand phen to dppz only induced a slight red shift of the absorption bands at < 450 nm. While all three complexes exhibited essentially the same emission energy, and the electronic configurations of the emitting states for **1-3** were the same (piq ligand-localized $^3\pi,\pi^*$ mixed with some ^{3}MLCT/^{3}LMCT characters) in toluene, the emitting state of **3** was the T$_2$ state. This difference resulted in a drastically reduced emission quantum yield and a somewhat shorter emission lifetime for **3** compared to those of **1** and **2**. In addition, the nature of the emitting T$_1$ state in **2** changed to the dppz core ligand-localized $^3\pi,\pi^*$/^{3}ILCT state in CH$_3$CN, which significantly reduced the emission quantum yield and lifetime of **2** in CH$_3$CN. Complexes **1-3** all displayed broad triplet excited-state absorption at 450-800 nm in toluene and acetonitrile. However, due to the different nature of the T$_1$ state for **3** in toluene, it exhibited much stronger TA signals at ca. 540 nm and in the NIR region with a much longer TA lifetime. Moreover, the dppz core ligand-localized $^3\pi,\pi^*$/^{3}ILCT nature of the T$_1$ state for **2** in CH$_3$CN increased the TA signals at 600-800 nm for **2**. Because of the strong triplet excited-state absorption of **1-3** at 532 nm, all three complexes manifested strong RSA at 532 nm, with the RSA trend following **3**>**2**>**1**, which paralleled the ratios of $\Phi_T\sigma_{ex}/\sigma_0$.

Comparison of the UV-vis absorption and transient absorption spectra of **2** and **3** to those of their corresponding complexes without the fluorenyl substituent, *i.e.* Ir(piq)$_2$dppz and Ir(piq)$_2$dppn, respectively, in CH$_3$CN revealed that fluorenyl substitution at the diimine ligand introduced a ^{1}ILCT and ^{3}ILCT states in the singlet and triplet excited states of the complexes. Although this new ^{1}ILCT state did not impact the low-energy absorption bands and the on-site of the lowest-energy absorption, the involvement of the ^{3}ILCT state significantly increased the triplet excited-state absorption in the NIR region (600-800 nm). This structural modification not only enhanced the RSA at 532 nm for **2** and **3**, but also made them potential broadband reverse saturable absorbers for broadband optical limiting applications.

Experimental section

Synthesis and characterization

All reagents and solvents were purchased from commercial sources and used directly unless otherwise mentioned. ^{1}H NMR spectra were recorded on a Bruker-400 spectrometer in CDCl$_3$ with tetramethylsilane (TMS) as the internal standard or in dimethyl sulfoxide-d$_6$ (DMSO-d$_6$). High resolution mass (HRMS) analyses were carried out on a Waters Synapt G2-Si mass spectrometer. Elemental analyses were conducted by NuMega Resonance Laboratories, Inc. in San Diego, California.

3,8-Dibromophenanthroline (**phen-2Br**) and 2-(9,9-di(2-ethylhexyl)-9H-fluoren-2-yl)-4,4,5,5-tetramethyl-1,3,2-dioxaborolane were prepared according to the reported methods.[57,58] Chlorobis(1-phenylisoquinoline)iridium(III) dimer ([Ir(piq)$_2$Cl]$_2$) was synthesized following the reported Nonoyama method from the commercially available ligand 1-phenylisoquinoline.[59] The diimine ligand 3,8-difluorenylphenanthroline was prepared by Suzuki coupling between 3,8-dibromophenanthroline (phen-2Br) and 2-(9,9-dioctyl-9H-fluoren-2-yl)-4,4,5,5-tetramethyl-1,3,2-dioxaborolane.[60] The synthesis and characterization data for complex **1** were reported previously.[25]

3,8-Dibromo-phen-5,6-dione (**phenBr2O2**). 3,8-Dibromo-phen (676 mg, 2.0 mmol) was added to an ice-cold mixture of 10 mL H$_2$SO$_4$ and 5 mL HNO$_3$ in one portion and then potassium bromide (408 mg, 3.4 mmol) was added in several portions to ensure that every portion of the added KBr was fully dissolved before the next portion was added. The mixture was kept stirring for additional 30 minutes before it was heated to 100 ^{o}C for 3 hours. The mixture was cooled to room temperature and then poured into icy water. NaOH was then added slowly to adjust the pH to ~ 6. The resulting suspension was filtered and dried in the oven. 340 mg yellow powder was afforded (yield: 46%) as the product. ^{1}H NMR (400 MHz, CDCl$_3$): δ 9.12 (d, J = 2.4 Hz, 2H), 8.59 (d, J = 2.4 Hz, 2H).

Compound **dppz-2Br**. Compound *o*-phenyldiamine (45 mg, 0.41 mmol) was added to the solution of phenBr2O2 (100 mg, 0.27 mmol) in 35 mL EtOH. The mixture was heated to reflux for 12 hours under argon. After evaporating the solvent, the crude product was purified by column chromatography (silica gel, eluent: CH$_2$Cl$_2$) to afford a pale yellow solid (90 mg, yield: 88%). ^{1}H NMR (400 MHz, CDCl$_3$): δ 9.77 (d, J = 2.4 Hz, 2H), 9.25 (d, J = 2.4 Hz, 2H), 8.39 (m, 2H), 7.98 (m, 2H).

Compound **dppn-2Br**. PhenBr2O2 (150 mg, 0.41 mmol) and 2,3-diaminonaphthalene (78 mg, 0.49 mmol) were mixed in 100 mL round bottle flask, and then 50 mL ethanol was added as the solvent. The mixture was brought to reflux for 16 hours under argon. The reaction mixture was allowed to cool down to room temperature and the suspension was filtered to collect the yellow solid with a nearly quantitative yield. NMR spectrum was unable to be collected because the poor solubility of the product.

Ligand **L2**. The literature procedure was followed for the synthesis of **L2**.[41] Compound **dppz-2Br** (66 mg, 0.15 mmol) and F8-borate (172 mg, 0.33 mmol) were mixed in a 100-mL Schleck Tube. Then 1,2-dimethoxyethane/ethanol/water (8 mL for each solvent) were added. The reaction mixture was vacuumed and back-filled with argon for three times. Then Pd(PPh$_3$)$_4$ (15 mg, 0.0025 mmol, 5%) and K$_2$CO$_3$ (400 mg, 3.0 mmol) were added under argon. The reaction mixture was kept at 110 ^{o}C for 72 hours in the absence of light. After the mixture was cooled down to room temperature, the solvent was removed under vacuum and the crude product was purified by column chromatography (silica gel, eluent: CH$_2$Cl$_2$) to afford a pale yellow oil (110 mg, yield: 67%). ^{1}H NMR (400 MHz, CDCl$_3$): δ 9.90

(s, 2H), 9.59 (s, 2H), 8.50-8.45 (m, 2H), 8.01-7.94 (m, 6H), 7.84 (d, J = 8.0 Hz, 2H), 7.47 (m, 2H), 7.37-7.29 (m, 6H), 2.14-2.10 (m, 8H), 0.94-0.69 (m, 60H).

Complex **2**. The Ir(III) dimer [Ir(piq)$_2$Cl]$_2$ (32 mg, 0.025 mmol), **L2** (50 mg, 0.05 mmol), and AgSO$_3$CF$_3$ (13 mg, 0.05 mmol) were added to a 50-mL round bottom flask, and then CH$_2$Cl$_2$ and MeOH (20/10 mL) were added as the solvent. The mixture was heated to reflux under argon atmosphere for 22 hours. When the mixture was cooled to room temperature, 100 mg NH$_4$PF$_6$ (0.62 mmol) was added and the mixture was stirred for another 3 hours at room temperature. The solvent was evaporated under vacuum and then the crude product was purified by column chromatography on silica gel with CH$_2$Cl$_2$/MeOH (v/v = 50/1) being used as the eluent to afford a red solid as the product (45 mg, yield: 48%). ^{1}H NMR (400 MHz, CDCl$_3$): δ 10.1 (m, 2H), 9.05 (s, 2H), 8.56-8.49 (m, 6H), 8.12 (m, 2H), 7.92-7.77 (m, 12H), 7.62-7.60 (m, 2H), 7.39-7.29 (m, 12H), 7.12-7.08 (m, 2H), 6.59-6.57 (m, 2H), 2.08-2.00 (m, 8H), 0.94-0.29 (m, 60H). ESI-HRMS calcd for [C$_{106}$H$_{110}$IrN$_6$]$^+$ (M-PF$_6$): 1659.8453, Found: 1659.8451. Anal calcd (%) for C$_{106}$H$_{110}$IrN$_6$PF$_6$•2H$_2$O: C, 69.14; H, 6.24; N, 4.56. Found: C, 69.11; H, 6.17; N 4.52.

Complex **Ir(piq)$_2$(dppn-2Br)**. In a 50-mL round-bottom flask was added iridium dimer [Ir(piq)$_2$Cl]$_2$ (84 mg, 0.065 mmol), dppn-2Br (65 mg, 0.133 mmol), and AgSO$_3$CF$_3$ (34 mg, 0.133 mmol). CH$_2$Cl$_2$ and MeOH (20/10 mL) were then added as the solvent. The system was heated to reflux under argon atmosphere for 24 hours. When the mixture was cooled to room temperature, 160 mg NH$_4$PF$_6$ (1 mmol) was added and the mixture was stirred for another 3 hours at room temperature. The solvent was evaporated under vacuum and then the crude product was purified by column chromatography on silica gel with CH$_2$Cl$_2$/MeOH (v/v = 30:1) as the eluent. The target complex was obtained as a red solid (120 mg, yield: 80%). ^{1}H NMR (400 MHz, CDCl$_3$): δ 9.94 (d, J = 2.0 Hz, 2H), 9.08 (s, 2H), 8.96 (m, 2H), 8.35 (d, J = 8.0 Hz, 2H), 8.26 (m, 2H), 8.01 (d, J = 2.0 Hz, 2H), 7.94-7.92 (m, 2H), 7.82-7.79 (m, 4H), 7.65-7.60 (m, 2H), 7.53 (d, J = 8.0 Hz, 2H), 7.48 (d, J = 8.0 Hz, 2H), 7.21 (t, J = 8.0 Hz, 2H), 7.00 (d, J = 8.0 Hz, 2H), 6.35 (d, J = 8.0 Hz, 2H).

Complex **3**. Complex **Ir(piq)$_2$(dppn-2Br)** (40 mg, 0.033 mmol), F8-borate (50 mg, 0.10 mmol) and K$_2$CO$_3$ (30 mg, 0.60 mmol) were mixed in an oven-dried Schleck tube. Then Pd(PPh$_3$)$_4$ (12 mg, 0.01 mmol) was added under argon atmosphere. Degassed THF (10 mL) and water (2 mL) were then added as the solvent. The mixture was further degassed before it was heated to reflux under argon atmosphere for 22 hours. When the mixture was cooled to room temperature, and 100 mg NH$_4$PF$_6$ (0.62 mmol) was added. The mixture was stirred for another 3 hours at room temperature. The solvent was evaporated under vacuum and then the crude product was purified by column chromatography on silica gel with CH$_2$Cl$_2$/MeOH (v/v = 50:1) being used as the eluent to give the desired product as an orange-red solid (20 mg, yield: 33%). ^{1}H NMR (400 MHz, CDCl$_3$): δ 10.1 (m, 2H), 9.18 (m, 2H), 9.06 (m, 2H), 8.47 (m, 4H), 8.31 (m, 2H), 7.94-7.73 (m, 16H), 7.44-7.34 (m, 12H), 7.12-7.08 (m, 2H), 6.59-6.57 (m, 2H), 2.08-2.00 (m, 8H), 0.94-0.29 (m, 60H). ESI-HRMS calcd for [C$_{110}$H$_{112}$IrN$_6$]$^+$ (M-PF$_6$): 1709.8590, Found:

1709.8628. Anal calcd (%) for C$_{110}$H$_{112}$IrN$_6$PF$_6$•H$_2$O: C, 70.53; H, 6.13; N, 4.49. Found: C, 70.66; H, 6.32; N 4.66.

Photophysical measurements

The solvents used for the photophysical studies were spectroscopic grade and purchased from VWR International and used without further purification. The ultraviolet-visible (UV-vis) absorption spectra were recorded on a Varian Cary 50 spectrophotometer. Steady-state emission spectra were measured on a Jobin-Yvon FluoroMax-4 fluorometer/phosphorometer. The emission quantum yields were determined by the relative actinometry in degassed solvents, in which [Ru(bpy)$_3$]Cl$_2$ in degassed CH$_3$CN (λ_{max} = 436 nm, Φ_{em} = 0.097)[61] was used as the reference.

The nanosecond transient difference absorption (TA) spectra and decays were measured in degassed toluene solutions on an Edinburgh LP920 laser flash photolysis spectrometer. The third harmonic output (355 nm) of a Nd:YAG laser (Quantel Brilliant, pulse width = 4.1 ns, repetition rate = 1 Hz) was used as the excitation source. Each sample was purged with argon for 40 min prior to measurement. The triplet excited-state absorption coefficients (ε_T) at the TA band maximums were determined by the partial saturation method.[52,53]

The reverse saturable absorption of **1**-**3** was studied by the nonlinear transmission experiment at 532 nm using a Quantel Brilliant laser as the light source. The pulse width of the laser was 4.1 ns, and the repetition rate was set to 10 Hz. All the complexes were dissolved in toluene or CH$_3$CN and the concentrations of the sample were adjusted to ensure that the linear transmission of all solutions was 80% at 532 nm in a 2-mm cuvette. The experimental setup and details were similar to those reported previously.[15] The radius of the laser beam waist at the focal plane was approximately 96 μm.

Computational methods

Geometry optimizations of **1**-**3** were carried out at the level of density functional theory (DFT) using PBE0 hybrid functional[62] and the mixed basis set of LANL2DZ[63] for Ir(III) and 6-31G* [64] for the remaining atoms. The absorption spectra were calculated using linear response time-dependent DFT (TDDFT) based on Davidson algorithm,[47-50] applying the same functional and the basis set as in the ground state calculations. The profiles of absorption spectra were obtained based on inhomogeneous Gaussian line-broadening of 0.08 eV to match the experimental absorption spectra. Both the geometry optimization and excited state calculations were performed via conductor-like polarizable continuum model (CPCM)[65,66] with toluene (ε_r = 2.38) being chosen as the solvent media for consistency with the experiments. All calculations used the Gaussian09 software package.[67]

Phosphorescence energies of **1**-**3** were computed based on the self-consistent optimization of the triplet spin state configuration at the ground state[68] and then using this triplet geometry as an input geometry for optimization of the excited triplet state applying the analytical gradient TDDFT.[54,55] This approach had been successfully applied to Ru(II)[56,69] and Ir(III)[70-72] complexes in our previous studies. However, it is known that the triplet state geometry optimization is highly sensitive to the

ARTICLE

initial guess of the trial wavefunction.[69,73,74] Starting with one of the three lowest triplet excitons as an initial guess for the emitting state, we were able to converge to several triplet excitons with different origins of $^3\pi,\pi^*$ and charge-transfer (^{3}CT) character in complex **3**. However, complexes **1** and **2** exhibited the same nature for their lowest triplet excitons. Complicated nature of the triplet potential energy surfaces in complex **3** provided conditions for populations of several low-energy excitons with different localization properties, resulting in lifetime difference between the emitting and transient absorbing states, which was probed experimentally.

The localization/delocalization character of the singlet and triplet exactions was obtained using natural transition orbital (NTO) analysis that allowed us to extract the charge density distribution of electron-hole pairs corresponding to each optical transition.[51] NTO procedure was performed using Gaussian09 software. The visualization of important NTOs was done via Chemcraft-1.7 software[75] using an isovalue of 0.02.

Conflicts of interest

There are no conflicts to declare.

Acknowledgements

Notes and references

1 Y. You and S. Y. Park, *Dalton Trans.*, 2009, 1267-1282.
2 G. Zhang, H. Zhang, Y. Gao, R. Tao, L. Xin, J. Yi, F. Li, W. Liu and J. Qiao, *Organometallics*, 2014, **33**, 61-68.
3 Q. Zhao, M. Yu, L. Shi, S. Liu, C. Li, M. Shi, Z. Zhou, C. Huang and F. Li, *Organometallics*, 2010, **29**, 1085-1091.
4 W. J. Finkenzeller and H. Yersin, *Chem. Phys. Lett.*, 2003, **377**, 299-305.
5 X. Yang, G. Zhou and W.-Y. Wong, *Chem. Soc. Rev.*, 2015, **44**, 8484-8575.
6 M. S. Lowry and S. Bernhard, *Chem. Eur. J.*, 2006, **12**, 7970-7977.
7 R. D. Costa, E. Ortí, H. J. Bolink, F. Monti, G. Accorsi and N. Armaroli, *Angew. Chem. Int. Ed.*, 2012, **51**, 8178-8211.
8 B. Elias, F. Shao and J. K. Barton, *J. Am. Chem. Soc.*, 2008, **130**, 1152-1153.
9 F. Shao and J. K. Barton, *J. Am. Chem. Soc.*, 2007, **129**, 14733-14738.
10 S. Sato, T. Morikawa, T. Kajino and O. Ishitani, *Angew. Chem. Int. Ed.*, 2013, **52**, 988-992.
11 Y. Lu, N. McGoldrick, F. Murphy, B. Twamley, X. Cui, C. Delaney, G. M. O.Maille, J. Wang, J. Zhao and S. M. Draper, *Chem. Eur. J.*, 2016, **22**, 11349-11356.
12 Y. Lu, J. Wang, N. McGoldrick, X. Cui, J. Zhao, C. Caverly, B. Twamley, G. M. O'Maille, B. Irwin, R. Conway-Kenny and S. M. Draper, *Angew. Chem. Int. Ed.*, 2016, **55**, 14688-14692.
13 L. He, Y. Li, C.-P. Tan, R.-R. Ye, M.-H. Chen, J.-J. Cao, L.-N. Ji and Z.-W. Mao, *Chem. Sci.*, 2015, **6**, 5409-5418.
14 S. P.-Y. Li, H.-W. Liu, K. Y. Zhang and K. K.-W. Lo, *Chem. Eur. J.*, 2010, **16**, 8329-8339.
15 C. Wang, L. Lystrom, H. Yin, M. Hetu, S. Kilina, S. A. McFarland and W. Sun, *Dalton Trans.*, 2016, **45**, 16366-16378.
16 L. Wang, S. Monro, P. Cui, H. Yin, B. Liu, C. G. Cameron, W. Xu, M. Hetu, A. Fuller, S. Kilina, S. A. McFarland and W. Sun, *ACS Appl. Mater. Interfaces*, 2019, **11**, 3629-3644.
17 B. Liu, S. Monro, L. Lystrom, C. G. Cameron, K. Colon, H. Yin, S. Kilina, S. A. McFarland and W. Sun, *Inorg. Chem.*, 2018, **57**, 9859–9872.
18 B. Liu, S. Monro, Z. Li, M. A. Jabed, D. Ramirez, C. G. Cameron, K. Colon, J. Roque III, S. Kilina, J. Tian, S. A. McFarland and W. Sun, *ACS Appl. Bio Mater.*, 2019, **2**, 2964-2977.
19 Y. Li, N. Dandu, R. Liu, L. Hu, S. Kilina and W. Sun, *ACS Appl. Mater. Interfaces.*, 2013, **5**, 6556-6570.
20 J. Massue, J. Olesiak-Banska, E. Jeanneau, C. Aronica, K. Matczyszyn, M. Samoc, C. Monnereau and C. Andraud, *Inorg. Chem.*, 2013, **52**, 10705-10707.
21 W. Sun, C. Pei, T. Lu, P. Cui, Z. Li, C. McCleese, Y. Fang, S. Kilina, Y. Song and C. Burda, *J. Mater. Chem. C*, 2016, **4**, 5059-5072.
22 K.-Y. Kim, R. T. Farley and K. S. Schanze, *J. Phys. Chem. B*, 2006, **110**, 17302-17304.
23 Y. Li, N. Dandu, R. Liu, Z. Li, S. Kilina and W. Sun, *J. Phys. Chem. C*, 2014, **118**, 6372-6384.
24 Z. Li, P. Cui, C. Wang, S. Kilina and W. Sun, *J. Phys. Chem. C*, 2014, **118**, 28764-28775.
25 L. Wang, P. Cui, S. Kilina and W. Sun, *J. Phys. Chem. C*, 2017, **121**, 5719-5730.
26 X. Zhu, P. Cui, S. Kilina and W. Sun, *Inorg. Chem.*, 2017, **56**, 13715-13731.
27 Z. Li, H. Li, B. J. Gifford, W. D. N. Peiris, S. Kilina and W. Sun, *RSC Adv.*, 2016, **6**, 41214-41228.
28 X. Zhu, L. Lystrom, S. Kilina and W. Sun, *Inorg. Chem.*, 2016, **55**, 11908–11919.
29 C. Pei, P. Cui, C. McCleese, S. Kilina, C. Burda and W. Sun, *Dalton Trans.*, 2015, **44**, 2176-2190.
30 R. Liu, N. Dandu, J. Chen, Y. Li, Z. Li, S. Liu, C. Wang, S. Kilina, B. Kohler and W. Sun, *J. Phys. Chem. C*, 2014, **118**, 23233-23246.
31 Y. Li, N. Dandu, R. Liu, S. Kilina and W. Sun, *Dalton Trans.*, 2014, **43**, 1724-1735.
32 Y. Fan, D. Ding and D. Zhao, *Chem. Commun.*, 2015, **51**, 3446-3449.
33 Y. Fan, J. Zhao, Q. Yan, P. R. Chen and D. Zhao, *ACS Appl. Mater. Interfaces*, 2014, **6**, 3122-3131.
34 H. Zhao, P. V. Simpson, A. Barlow, G. J. Moxey, M. Morshedi, N. Roy, R. Philip, C. Zhang, M. P. Cifuentes and M. G. Humphrey, *Chem. Eur. J.*, 2015, **21**, 11843-11854.
35 G.-J. Zhou and W.-Y. Wong, *Chem. Soc. Rev.*, 2011, **40**, 2541-2566.
36 S. Hirata, K. Totani, T. Yamashita, C. Adachi and M. Vacha, *Nat. Mater.*, 2014, **13**, 938-946.
37 W. Blau, H. Byrne, W. M. Dennis and J. M. Kelly, *Opt. Commun.*, 1985, **56**, 25-29.
38 D. J. Harter, M. L. Shand and Y. B. Band, *J. Appl. Phys.*, 1984, **56**, 865-868.
39 Y. Sun, L. E. Joyce, N. M. Dickson and C. Turro, *Chem. Commun.*, 2010, **46**, 2426-2428.
40 S. P. Foxon, M. A. H. Alamiry, M. G. Walker, A. J. H. M. Meijer, I. V. Sazanovich, J. A. Weinstein and J. A. Thomas, *J. Phys. Chem. A*, 2009, **113**, 12754-12762.
41 T. Shigehiro, Y. Kawai, S. Yagi, T. Maeda, H. Nakazumi and Y. Sakurai, *Chem. Lett.*, 2015, **44**, 288-290.

42   J. Frey, T. Kraus, V. Heitz and J.-P. Sauvage, *Chem. Eur. J.*, 2007, **13**, 7584-7594.

43   W.-J. Li, H.-M. Wu, Y.-B. Li, C.-P. Hu, M.-D. Yi, L.-H. Xie, L. Chen, J.-F. Zhao, X.-H. Zhao, N.-E. Shi, Y. Qian, C. Wang, W. Wei and W. Huang, *Tetrahedron*, 2012, **68**, 8216-8221.

44   S. Itoh, K. Nii, M. Mure and Y. Ohshiro, *Tetrahedron Lett.*, 1987, **28**, 3975-3978.

45   K. Ritter, C. Pehlken, D. Sorsche and S. Rau, *Dalton Trans.*, 2015, **44**, 8889-8905.

46   Y. Lu, N. McGoldrick, F. Murphy, B. Twamley, X. Cui, C. Delaney, G. M. Ó. Máille, J. Wang, J. Zhao and S. M. Draper, *Chem. Eur. J.*, 2016, **22**, 11349-11356.

47   M. E. Casida, in Time-Dependent Density-Functional Response Theory for Molecules, ed. D. P. Chong, World Scientific, Singapore, 1995, **1**, 155–192.

48   L. Künne, *Z. Phys. Chem.*, 1998, **204**, 263-264.

49   R. Bauernschmitt and R. Ahlrichs, *Chem. Phys. Lett.*, 1996, **256**, 454-464.

50   E. R. Davidson, *J. Comput. Phys.*, 1975, **17**, 87-94.

51   R. L. Martin, *J. Chem. Phys.*, 2003, **118**, 4775-4777.

52   I. Carmichael and G. L. Hug, *J. Phys. Chem. Ref. Data.*, 1986, **15**, 1-250.

53   P. Shao, Y. Li, A. Azenkeng, M. Hoffmann, W. Sun, *Inorg. Chem.*, 2009, **48**, 2407-2419.

54   C. van Caillie and R. D. Amos, *Chem. Phys. Lett.*, 2000, **317**, 159-164.

55   F. Furche and R. Ahlrichs, *J. Chem. Phys.*, 2002, **117**, 7433-7447.

56   L. Wang, H. Yin, M. A. Jabed, M. Hetu, S. Monro, C. Wang, S. Kilina, S. A. McFarland and W. Sun, *Inorg. Chem*., 2017, **56**, 3245-3259.

57   M. Karnahl, S. Krieck, H. Görls, S. Tschierlei, M. Schmitt, J. Popp, D. Chartrand, G. S. Hanan, R. Groarke, J. G. Vos and S. Rau, *Eur. J. Inorg. Chem.*, 2009, **2009**, 4962-4971.

58   Q. Wang, Y. Qu, H. Tian, Y. Geng and F. Wang, *Macromol.*, 2011, **44**, 1256-1260.

59   N. Matsuo, *Bull. Chem. Soc. Jap.*, 1974, **47**, 767-768.

60   X. Zeng, M. Tavasli, I. F. Perepichka, A. S. Batsanov, M. R. Bryce, C.-J. Chiang, C. Rothe and A. P. Monkman, *Chem. Eur. J.*, 2008, **14**, 933-943.

61   K. Suzuki, A. Kobayashi, S. Kaneko, K. Takehira, T. Yoshihara, H. Ishida, Y. Shiina, S. Oishi and S. Tobita, *Phys. Chem. Chem. Phys.*, 2009, **11**, 9850-9860.

62   J. P. Perdew, K. Burke and M. Ernzerhof, *Phys. Rev. Lett.*, 1996, **77**, 3865-3868.

63   P. J. Hay and W. R. Wadt, *J. Chem. Phys.*, 1985, **82**, 270–283.

64   C. Adamo and V. Barone, *J. Chem. Phys.*, 1999, **110**, 6158–6170.

65   M. Cossi, N. Rega, G. Scalmani and V. Barone, *J. Comput. Chem.*, 2003, **24**, 669-681.

66   V. Barone and M. Cossi, *J. Phys. Chem. A*, 1998, **102**, 1995-2001.

67   M. J. Frisch, G. W. Trucks, H. B. Schlegel, G. E. Scuseria, M. A. Robb, J. R. Cheeseman, G. Scalmani, V. Barone, B. Mennucci, G. A. Petersson, H. Nakatsuji, M. Caricato, X. Li, H. P. Hratchian, A. F. Izmaylov, J. Bloino, G. Zheng, J. L. Sonnenberg, M. Hada, M. Ehara, K. Toyota, R. Fukuda, J. Hasegawa, M. Ishida, T. Nakajima, Y. Honda, O. Kitao, H. Nakai, T. Vreven, J. A. Montgomery Jr., J. E. Peralta, F. Ogliaro, M. Bearpark, J. J. Heyd, E. Brothers, K. N. Kudin, V. N. Staroverov, R. Kobayashi, J. Normand, K. Raghavachari, A. Rendell, J. C. Burant, S. S. Iyengar, J. Tomasi, M. Cossi, N. Rega, J. M. Millam, M. Klene, J. E. Knox, J. B. Cross, V. Bakken, C. Adamo, J. Jaramillo, R. Gomperts, R. E. Stratmann, O. Yazyev, A. J. Austin, R. Cammi, C. Pomelli, J. W. Ochterski, R. L. Martin, K. Morokuma, V. G. Zakrzewski, G. A. Voth, P. Salvador, J. J. Dannenberg, S. Dapprich, A. D. Daniels, Ö. Farkas, J. B. Foresman, J. V. Ortiz, J. Cioslowski and D. J. Fox, Guassian09, Revision A.1, Gaussian Inc., Wallingford CT, 2009.

68   S. Kilina, D. Kilin and S. Tretiak, *Chem. Rev.*, 2015, **115**, 5929–5978.

69   E. Badaeva, V. V. Albert, S. Kilina, A. Koposov, M. Sykora and S. Tretiak, *Phys. Chem. Chem. Phys.*, 2010, **12**, 8902-8913.

70   B. Liu, L. Lystrom, S. Kilina and W. Sun, *Inorg. Chem.*, 2019, **58**, 476-488.

71   B. Liu, L. Lystrom, S. L. Brown, E. K. Hobbie, S. Kilina and W. Sun, *Inorg. Chem.*, 2019, **58**, 5483-5493.

72   B. Liu, L. Lystrom, S. Kilina and W. Sun, *Inorg. Chem.*, 2017, **56**, 5361-5370.

73   E. R. Batista and R. L. Martin, *J. Phys. Chem. A*, 2005, **109**, 9856-9859.

74   E. Jakubikova, W. Z. Chen, D. M. Dattelbaum, F. N. Rein, R. C. Rocha, R. L. Martin, and E. R. Batista, *Inorg. Chem.*, 2009, **48**, 10720-10725.

75   G. A. Zhurko and D. A. Zhurko, ChemCraft 1.7, http://www.chemcraftprog.com.

New J. Chem.

ARTICLE

Table of Contents Entry

Fluorenyl substitution at the diimine ligand broadened the excited-state absorption to near-IR, and enhanced reverse saturable absorption at 532 nm for the cationic Ir(III) complexes.